Journal of Power Sources 194 (2009) 588–600

Contents lists available at ScienceDirect

Journal of Power Sources

journal homepage: www.elsevier.com/locate/jpowsour

Review

A review of platinum-based catalyst layer degradation in proton exchange membrane fuel cells

Shengsheng Zhang[a], Xiao-Zi Yuan[a], Jason Ng Cheng Hin[a], Haijiang Wang[a,*], K. Andreas Friedrich[b], Mathias Schulze[b]

[a] Institute for Fuel Cell Innovation, National Research Council of Canada, Vancouver, B.C., Canada V6T 1W5
[b] Institute of Technical Thermodynamics, German Aerospace Center, Pfaffenwaldring 38-40, 70569 Stuttgart, Germany

ARTICLE INFO

Article history:
Received 8 April 2009
Received in revised form 19 June 2009
Accepted 22 June 2009
Available online 30 June 2009

Keywords:
PEM fuel cells
Durability
Catalyst layer
Degradation mechanism

ABSTRACT

Catalyst layer degradation has become an important issue in the development of proton exchange membrane (PEM) fuel cells. This paper reviews the most recent research on degradation and durability issues in the catalyst layers including: (1) platinum catalysts, (2) carbon supports, and (3) Nafion ionomer and interfacial degradation. The review aims to provide a clear understanding of the link between microstructural/macrostructural changes of the catalyst layer and performance degradation of the PEM fuel cell fueled with hydrogen under normal operating or accelerated stress conditions. In each section, different degradation mechanisms and their corresponding representative mitigation strategies are presented. Also, general experimental methods are classified and various investigation techniques for evaluating catalyst degradation are discussed.

Contents

* Corresponding author. Tel.: +1 604 221 3038; fax: +1 604 221 3001.
E-mail address: Haijiang.Wang@nrc-cnrc.gc.ca (H. Wang).

0378-7753/$ – see front matter.
doi:10.1016/j.jpowsour.2009.06.073

1. Introduction

Other than cost, durability is another key issue for the commercialization of proton exchange membrane (PEM) fuel cells. So far, the operational lifetime for real life applications does not satisfy the requirements for state-of-the-art technologies, e.g., 5000 h for cars, 20,000 h for buses, and 40,000 h for stationary applications [1]. To improve the lifetime of PEM fuel cells, a profound understanding of failure modes for each component as well as the corresponding mitigation strategies is urgently required. In the past few years, numerous papers have been published that focus on the degradation issues of PEM fuel cells. As a result, studies have shown that several factors can affect the durability of a PEM fuel cell. These factors include PEM thinning [2–4], catalyst layer (CL) degradation due to platinum sintering [5,6] or carbon support corrosion [7,8], and gas diffusion layer (GDL) degradation [9,10]. Among these, CL degradation is one of the most critical factors. More and more experimental results have shown severe catalyst degradation in both automotive and stationary applications. Increasing CL durability is becoming a major challenge and a growing focus of research attention in PEM fuel cell durability studies.

In the PEM fuel cell CL, the catalysts can be classified into three groups based on the active component: Pt-based catalyst (Pt supported on carbon or other supports); Pt-based catalysts that are modified or alloyed by other metals such as Cr [11], Cu [12], Co [13], and Ru [14]; and non-Pt-based catalysts such as non-noble metals [15] and organometallic complexes [16]. Fig. 1 lists commonly used or studied catalysts for PEM fuel cells as well as their advantages and disadvantages. Although a variety of catalysts are being investigated so far, Pt/C and Pt-modified or alloyed catalysts are still the most popular catalyst in use due to their low overpotential and high catalytic activity for the hydrogen oxidation reaction (HOR) and the oxygen reduction reaction (ORR) as well as their ability to withstand the harsh acidic environment inside a PEM fuel cell.

In recent years, quite a few excellent reviews on PEM fuel cell catalyst materials and their stability can be found in open literature. For example, for the cathode catalyst, Yu and Ye [17] reviewed the activity and durability issues of Pt/C catalytic cathode in PEM fuel cells. Gasteiger et al. [18] reviewed the activities and requirements of Pt catalysts, Pt-alloy catalysts and non-Pt catalysts, especially for automotive applications. Also, Antolini et al. [19] introduced the stability of Pt-M (M = first row transition metal) alloy catalysts compared to traditional Pt/C catalysts. Shao et al. [20] summarized the degradation mechanisms of Pt-based catalyst, which mainly focused on degradations of carbon and catalytic metals and especially under harsh working conditions. With respect to the approaches for improving catalyst durability, the authors introduced the highly graphitized carbons and alloyed Pt. There are also numerous other papers that have been published on performance degradation and failure mechanisms of PEM fuel cells where catalyst degradation is introduced as a very important issue. For instance, Borup et al. [21] published a very comprehensive review paper on the fundamental aspects of PEMFC durability and degradation, including operational effects and different components degradation (membrane, electrocatalyst, and gas diffusion layer). Rama et al. [22] summarized the catalyst resulted activation losses and classified them into platinum catalysts, geometric structure of the CLs, and carbon supports. Schmittinger and Vahidi [23] presented the effects of corrosion and contamination of the electrocatalyst in both the anode and cathode sides. Zhang et al. [24] placed extra emphasis on platinum and carbon degradation under different accelerated stressors in PEM fuel cells.

All these reviews contribute to the understanding and improvement of PEM fuel cell degradation issues. However, the topics included in this area are much broader than the knowledge being revealed so far. A sufficient understanding of Pt-based catalysts and the whole CL is still required due to their significant importance in PEM fuel cell development. On the basis of the previous work, this paper reviews Pt, carbon support, ionomer, and interfacial degradations of the CL with focuses on the physical and chemical/electrochemical changes of the entire CL on microscopic and macroscopic scales, and how these changes deteriorate the performance of PEM fuel cells. Other than Pt and carbon degradations, ionomer and interfacial degradations have not been thoroughly reviewed even though they are drawing much attention in recent studies. Also, this review combines the mitigation strategies with degradation mechanisms related to different constituents of the CL, and introduces

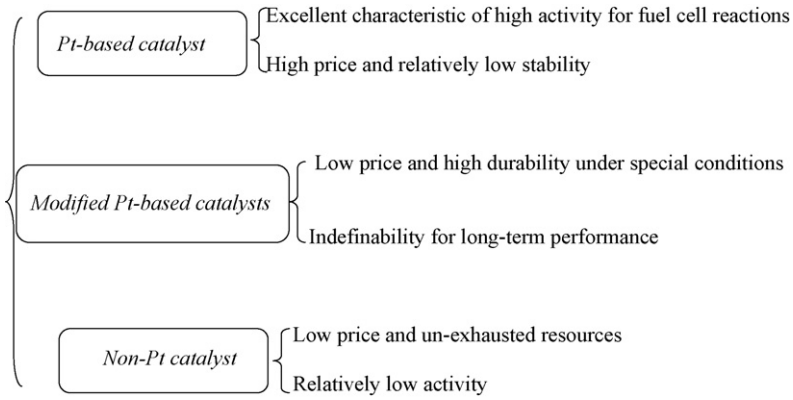

Fig. 1. General comparison of three types of catalyst for PEM fuel cells.

novel research methods as well as newly emerged experimental instruments.

2. Methodologies in catalyst layer degradation research

2.1. Experimental approaches

Two basic methods are commonly used to investigate the durability of PEM fuel cell systems and their components: The life test and the accelerated stress test (AST). Undoubtedly the most reliable way to assess the tolerance of a fuel cell and its components is to simulate real steady state or dynamic state operating conditions. For example, Wang et al. [25] operated a fuel cell at a current density of 160 mA cm^{-2} for 2250 h. The characterization by transmission electron microscope (TEM) revealed that, after the life test, the average diameter of Pt particles increased from 2.6 nm of a fresh electrode to 5.1 nm for the anode and 7.3 nm for the cathode. Accordingly, the calculated utilization of the cathodic and anodic catalyst decreased 18.6% and 13.1% respectively. This experiment provides reliable information for catalyst degradation of PEM fuel cells under practical operating conditions; however, the process is quite time-consuming and costly.

Because of the disadvantages of regular life tests, AST is becoming more popular for exploring durability issues, including CL degradation in PEM fuel cells. AST significantly reduces the time of experiments for lifetime evaluation and degradation mode analysis and can be conducted on either an entire fuel cell (in situ) or an electrochemical half-cell (ex situ) system. One of the most frequently used accelerated stressors for catalyst degradation is controlled potential. This includes: (1) potential cycling from low to high potentials, (2) square (or triangular)-wave potential control, and (3) steady-state potential control at specified voltage values. Fig. 2 shows some voltage cycling profile examples investigated by Mitsushima et al. [6]. Uchimura and Kocha [26] also discussed the impact of potential cycling profiles on PEM fuel cell durability and explained that PtO_x dissolution plays an important role in contributing to CL degradation. Potential cycling simulates and simplifies the severe degradation that occurs during the operation of PEM fuel cells, which is the major concern for automotive applications.

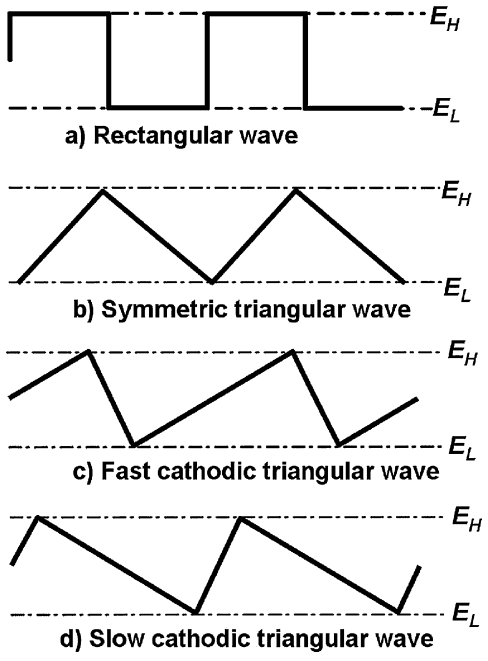

Fig. 2. Potential cycling profiles in durability testing experiments (Adapted from Ref. [6] with permission.)

Compared with in situ entire cell or stack operation, ex situ half-cell system testing in an aqueous acid solution (H_2SO_4 or $HClO_4$) has several advantages. Ex situ testing uses more simplified equipment and isolates the catalyst from other adjoining components. This avoids potentially confusing effects during the degradation evaluation. For instance, Yoshida et al. [27] carried out potential cycling between 0.6 and 1.2 V vs. RHE (Reversible Hydrogen Electrode) at a scan rate of 300 mV s^{-1} for 10,000 cycles to evaluate the Pt catalyst durability in a 3-electrode system in an H_2SO_4 solution. They found that, for smaller particles, the Pt parameters, such as coordination number and Pt–Pt band distance clearly changed with increasing cycling numbers, while those for larger Pt particles were relatively stable. Other groups [28,29] have proven similar trends in the effects of particle sizes during different potential oriented experiments. For this particle size effect, Bi and Fuller [30] proposed a physics-based Pt/C catalyst degradation model and explained that the high electrochemical dissolution of smaller Pt particles was a main reason for the shrinkage of small Pt particles during the potential cycling test. The disadvantage for electrochemical half-cell test comes from the difficulty of simulating real fuel cell operating conditions. From a practical point of view, an actual fuel cell test is the ultimate evaluation method for catalyst innovation.

2.2. Diagnostic tools

With the development of fuel cell technology, many different investigative tools, including electrochemical and physical/chemical methods, have become available that elucidate CL degradation. These methods provide valuable information on morphology (surface or cross section of the CL, size distribution of the catalyst particles), elemental content and distribution, atomic structure of the local particles inside the CL, and electrochemical characteristics of the CL in fuel cell systems. Table 1 summarizes the general investigative tools employed in the latest catalyst degradation research. The most frequently used tools can be classified into three categories: morphology observation, electrochemical diagnosis, and other analytical techniques.

2.2.1. Morphology observation

With the help of TEMs, the morphology changes of particles in the micro- and nano-scale can be observed after both in situ and ex situ aging processes. The scarcity of this diagnostic method is that most TEM detecting is destructive and limited to random observation and post analysis. In a recent research, by impregnating a TEM finder grid with the catalyst suspension and connecting it in parallel to the rotating disk electrode (RDE) as a second working electrode, Mayrhofer et al. [31] observed the degradation of the same catalyst region before and after the potential treatment, which is a progress compared with the conventional destructive TEM investigation.

Scanning electron microscopy (SEM) can be used to detect the surface condition, thickness and interfacial changes of the CL, as well as the elemental distribution changes when combined with energy dispersive spectroscopy (EDS).

Besides TEM and SEM, other morphology observation techniques have also been used in CL investigation. For example, Siroma et al. [32] observed the stability of glassy carbon substrate and high oriented pyrolytic graphite (HOPG) by using an atomic force microscope (AFM). Bussian et al. [33] also investigated the electrochemically active area of a PEM fuel cell using a conductive probe atomic force microscopy (CP-AFM), which provided a quantitative measure of the spatial distribution of electrochemically active aqueous domains in the cell. Inaba et al. [34] characterized Pt/C catalyst agglomeration with different loading densities on glassy carbon by using optical micrography. Garzon et al. [35] and Lau et al. [36]

Table 1
Physical/chemical and electrochemical investigation methods employed during the catalyst degradation research.

	Technologies	Characteristics	Information of the catalyst layer	References
Physical/chemical methods	TEM (transmission electron microscopy)	Morphology or Pt distribution analysis	Topography investigation and particle size distribution	[28,31,40,44,45,48,58,66,73]
	SEM or FEG-SEM or SEM-EDS (scanning electronic microscopy or Field-emission gun scanning electron microscopy or scanning electron microscopy combined with energy dispersive spectroscopy)		Topography investigation and elemental distribution analysis of a cross section of an MEA or CL	[32,38,44,45,48,57,73]
	AFM (atomic force microscopy) or CP-AFM (conductive probe atomic force microscopy)		Morphology of the surface of the carbon substrate	[32,33]
	Optical micrography		Dispersion of Pt/C catalyst on glassy carbon disk electrodes	[34]
	3-D X-ray CT (3D X-ray computer tomography)		Investigate changes in the internal morphology, Pt distribution and carbon content, etc.	[35,36]
	EPMA (electron probe micro-analysis)		Characterize the Pt content through the cross-section of the MEA	[66,70]
	AAS (atomic adsorption spectroscopy)	Elemental content analysis	Investigate the Pt content in the Pt/C catalyst	[38]
	ICP or ICP-AES or ICP-MS (inductively coupled plasma or inductively coupled plasma combined with atomic emission spectrometry or inductively coupled plasma combined with mass spectrometry)		Investigate the amount of metal content	[44,57,62]
	TGA-MS (thermal gravimetric analysis coupled with on-line mass spectrometry)		Characterize the oxygen content of electrochemically oxidized Vulcan carbon support	[78]
	UV (ultraviolet spectroscopy)		Detect the presence of Pt^{z+} ionic species (z = 2,4) in decantation solution of membrane	[45]
	XAS (X-ray absorption spectroscopy)	Atomic structure analysis	Give information about the atomic structure of the catalyst, mainly of the surface atoms	[27]
	XPS (X-ray photoelectron spectroscopy)		Surface oxygen content or electronic structure change of other surface elements	[37,43,57]
	LRS (laser Raman spectroscopy)		Detect the degree of structural disorder of carbon	[40]
	XRD (X-ray diffraction)		Pt particle average sizes and crystallinity of alloy materials analysis	[31,37,39,45,60]
Electrochemical methods	IV (polarization curve)	Potential or current scanning	Characterize cell performance by potential vs. current density under specialized conditions	[39,40,44,57]
	LSV (linear sweep voltammetry)		Obtain some detailed information about the degradation mechanism by position shift of the potential peak	[43]
	CV (cyclic voltammetry)	CV based scanning	Determine the ECSA of Pt by hydrogen adsorption	[31,38,40,45,57,60,66,73]
	COSV (CO-stripping voltammetry)		Determine the ECSA of Pt by CO oxidation	[31,37,57,45]
	EIS (electrochemical impedance spectroscopy)	Impedance	Characterize the polarization resistance (especially for ohmic resistance and charge transfer resistance)	[28,62,44]

described the applications and advantages of the multiscale 3D X-ray computer tomography (X-ray CT) systems for non-invasive characterization of the CL and other components when the fuel cell was subjected to different ASTs. Electron probe micro-analyzers (EPMA) were also employed to obtain surface images and cross-sectional element distribution of Pt for different ASTs, and proved to be sensitive in obtaining useful CL degradation information [66,70]. These newly emerged techniques with different resolutions and advantages are valuable in characterizing morphology alteration and element migration, as well as particle agglomeration within the CL, which helps better understand the CL degradation mechanisms.

2.2.2. Electrochemical diagnosis

The electrochemical surface area (ECSA) is a vital parameter for evaluation of catalyst performance. It can be calculated by the charge area under H-desorption on the smooth Pt measured by cyclic voltammetry (CV) and the catalyst loading in the CL. Both in situ (in a fuel cell) and ex situ (in a half-cell) CV curves are useful for assessing the catalyst performance by comparing the ECSA

value. CO-stripping voltammograms (COSVs) can also give hydrogen adsorption/desorption waves for the ECSA calculation [37]. Meanwhile, CV curves can provide information about the oxygen reduction activity by the shift in oxygen reduction potential [38,39] and carbon properties by the double layer charging current [40].

Electrochemical impedance spectroscopy (EIS) is another important diagnostic tool that has been widely used in PEM fuel cell research. For CL investigations, catalyst surface area, catalyst loading, and catalyst utilization can all be characterized with the data obtained from EIS measurements [41]. In addition, polarization curves (*IV* curves), both steady state and non-steady state [42], are the most frequently employed nondestructive tool used to characterize fuel cell performance. Several valuable parameters about the catalyst performance can be derived from these curves. For example, mass activity of the Pt catalyst can be defined as the current at 0.90 V vs. RHE (IR-free) per unit Pt weight ($A\,g^{-1}$) from *IV* curves. According to Shao et al.'s [43] publication, linear sweep voltammetry (LSV) can also be carried out on Pt/C catalysts to obtain information on degradation mechanisms (e.g., different surface oxide formations) under different accelerated conditions.

2.2.3. Other analytical techniques

Except for the morphology observation and electrochemical diagnosis, elemental and atomic structure analysis techniques are useful diagnostic tools to quantitatively characterize the microstructural/macrostructural changes of the CL during degradation.

For elemental content analysis, inductively coupled plasma (ICP) and atomic adsorption spectroscopy (AAS) can be used to investigate the Pt content change in the CL [38,44]. Also, Guilminot et al. [45] used ultraviolet spectroscopy (UV) successfully to detect the presence of Pt^{z+} ionic species. In terms of carbon support characterization, mass spectrometer (MS) or gas chromatograph (GC) are both effective tools to estimate the total amount of surface oxygen on carbon when combined with thermal desorption method [78].

For atomic structure analysis, X-ray diffraction (XRD) and X-ray photoelectron spectroscopy (XPS) are the most commonly used techniques to characterize the average Pt particle size and surface electronic structure change during the degradation process [31,37,39,45]. According to a recent report by Yoshida et al. [27], X-ray absorption spectroscopy (XAS) was carried out to obtain crucial information for atomic/electronic structure of the surface Pt. The results revealed that the local Pt structure of a Pt/C catalyst was inherent upon the particle size, a vital parameter that should lead to a difference in the electrochemical properties of Pt catalyst. The authors also derived the local structural parameters, coordination number, and Pt–Pt bond distance from extended X-ray absorption fine structure (EXAFS) oscillations. In addition, laser Raman spectroscopy (LRS) [40] has also been conducted in detecting the carbon structural disorder degree for CL degradation research in PEM fuel cells. Except for the broad band at ca. 1600 cm^{-1} assigned to the ideal graphite, the presence of another band at ca. 1350 cm^{-1} proved the existence of disordered graphite in the CL after high potential holding test.

3. Platinum degradation

Under a combination of different aggressive conditions (such as nano-scale particles, strong acidic environments, oxidizing conditions, reactive intermediates, durative flow of liquid and gas, high electric currents, and large potential gradients), the CL components tend to experience subtle changes and function losses during the operation of PEM fuel cells. For example, Pourbaix diagrams show that Pt is unstable at a potential range of 1.0–1.2 V vs. SHE (Standard Hydrogen Electrode) and at a pH of less than or equal to 1 [46]. These imperceptible changes will accumulate and result in a gradual decline in power output during the long-term operation of a PEM fuel cell.

3.1. Platinum degradation mechanisms

Direct reasons for Pt catalyst degradation include: (1) Pt particle agglomeration and particle growth, (2) Pt loss and redistribution, and (3) poisonous effects aroused by contaminants. All these effects will lead to either a loss of effective catalytic active sites or a loss of electronic contact with conductors, resulting in apparent activity loss in the CL during long-term operation.

3.1.1. Platinum agglomeration and particle growth

As demonstrated by many researchers, agglomeration and particle growth of the nanostructure of Pt is the most dominant mechanism for catalyst degradation in PEM fuel cells. First of all, it is believed that nano-sized structural elements are able to show size-dependant properties different from bulk elements [47]. Nanoparticles have the inherent tendency to agglomerate into bigger particles to reduce the high surface energy. As particles grow, their surface energy decreases and the growth process slows. The preparation method of the membrane electrode assembly (MEA) could be a cause of agglomeration and particle growth. This can be proven by examining the agglomeration of Pt particles in fresh MEAs [44,45,48]. However, during long-term or accelerated stress tests, the Pt/C catalysts can experience more severe agglomeration compared to normal inherit nano-scale Pt particle agglomeration. Ferreira et al. [49] analyzed degraded MEAs after 2000 h of operation under open-circuit voltage (OCV) in a H_2/air cell and explained that small Pt particles dissolve in the ionomer phase and redeposit on larger particles that are separated from each other by a few nanometers, forming a well-dispersed catalyst, called "Ostwald ripening". Virkar and Zhou [50] explained that Ostwald ripening, involving coupled transport of electrically charged species, is the main reason for particle growth in Pt/C catalysts, where the Pt is transported through the liquid and/or through the ionomer and the electrons through the carbon support. Other groups [31,48] believed that two other mechanisms are predominately responsible for degradation during the potential cycling process: (1) Pt particles detaching from the support and dissolving into the electrolyte without re-deposition, and/or (2) a combination of Pt particle coalescence and Pt solution/re-precipitation within the solid ionomer.

Whatever mechanism the particle growth follows, dissolution of Pt is an important step during the catalyst degradation process. The lower the Pt ion concentration, the lower the degradation kinetics for the Pt/C catalyst. Different electrode aging process may reveal different dissolution reactions taking place at the anode and the cathode. Using the rotating ring-disk electrode (RRDE) experiment following different sweep protocols, Kawahara et al. [51] proved that for a slow anodic triangular wave sweep, the Pt dissolution mechanism is $Pt \rightarrow Pt^{4+} + 4e^-$ or $PtO_2 + 4H^+ \rightarrow Pt + 2H_2O$. While for a cathodic sweep, the Pt dissolution mechanism is $PtO_2 + 4H^+ + 2e^- \rightarrow Pt^{2+} + 2H_2O$ with a charge transfer number of ca. 2.

Potential values also play an important role during the Pt degradation process. Higher potentials can accelerate Pt dissolvability. Wang et al. [52] suggested that the concentration of dissolved Pt increased monotonically from 0.65 to 1.1 V, and then decreased at potentials higher than 1.1 V due to the formation of a protective oxide film. Therefore, the potential limit for Pt catalyst degradation is generally lower than 1.0 V to avoid the possibility of carbon support corrosion. Yoda et al. [40] also proposed that the Pt electrocatalysts were dissolved even under standard operating conditions.

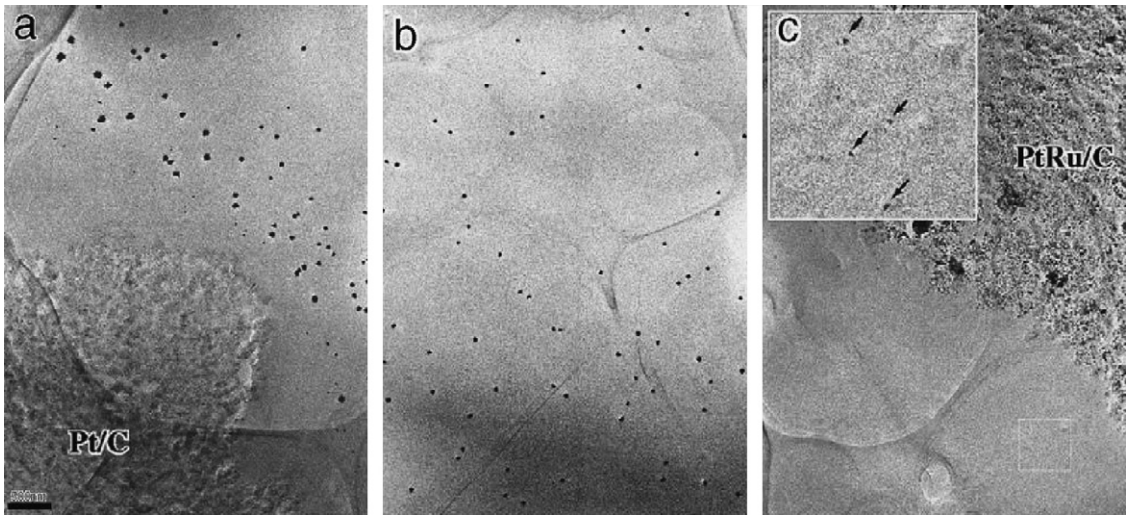

Fig. 3. Cross-sectional TEM images of a MEA after 1.0 V potential holding for 87 h, (a) near the interface of cathode CL and PEM, (b) PEM 10 μm from the CL, and (c) near the interface of anode CL and PEM (From Ref. [58] with permission.)

In addition, the agglomeration of Pt can also be affected by many other operating conditions such as temperature [40,53,54] or relative humidity [5,53,55].

3.1.2. Platinum loss and migration

Pt loss during operation is another major source of CL degradation. This can be caused by many factors such as Pt dissolution and wash-out. Luo et al. [38] conducted an experiment involving a 10-cell stack operating for 200 h under ambient humidity, ambient pressure and 60 °C. Pt content in the Pt/C CL was determined by AAS. The results showed that the Pt content was only 13.5% compared to the original value of 20%, which proved that there are serious Pt losses during the aging process. By weighing and using inductively coupled plasmacombined with mass spectrometer (ICP-MS), respectively, Mitsushima et al. [6] and Ball et al. [56] also measured Pt loss from the Pt/C catalyst in acidic electrolyte systems after potential cycling.

Pt migration within MEA has been observed to have the same effect as Pt loss. Many groups have reported the presence of Pt particles inside the PEM as well as enrichment of Pt in the CL/PEM interface under different conditions [29,45,49,57]. Fig. 3 shows Pt catalyst particles observed within the PEM and near the CL/PEM interface after degradation [58]. These Pt particles originate from the dissolved Pt species, which diffuse in the ionomer phase and subsequently precipitate in the ionomer phase of the electrode or in the membrane. The precipitation occurs via the reduction of Pt ions by hydrogen that has crossed over from the anode, and thus it is called the "micrometer-scale diffusion process". The redistribution of Pt nano-particles is actually a complex process involving (1) Pt dissolution, (2) formation of Pt^{z+} species, and (3) reduction to Pt particles by the crossover H_2 from anode to cathode. Considering the potential effect on Pt dissolution, the process of Pt dissolution most likely occurs on the cathode side. Darling and Meyers' [59] three-step dissolution model for Pt particles in the CL under stressed environments can be a good explanation of the Pt dissolution process:

$$\text{Platinum dissolution}: \ Pt_{(s)} \rightarrow {Pt_{(*)}}^{2+} + 2e^- \quad (1)$$

$$\text{Platinum oxide formation}: \ Pt_{(s)} + H_2O \rightarrow PtO_{(s)} + 2{H_{(*)}}^{+} + 2e^- \quad (2)$$

$$\text{Platinum oxide dissolution}: \ PtO_{(s)} + 2{H_{(*)}}^{+} \rightarrow {Pt_{(*)}}^{2+} + H_2O \quad (3)$$

where (*) denotes ionic species present in water or in the ionomer phase.

In the second stage, faster electro-oxidation of Pt into Pt^{z+} is also possible under higher potentials. Guilminot et al. [45] observed simultaneous Pt^{2+} and Pt^{4+} by ultraviolet (UV) detection, which proved the high mobility of Pt contained species. Also, the transport of Pt ions can be facilitated by the presence of species contained counter ions, such as F^- or $SO_x{}^-$ [57]. The migration direction of the species may cross over from the cathode to the anode through the membrane driven by electro-osmotic drag and chemical diffusion.

In the third stage, the Pt^{z+} species are chemically and electrochemically reduced to Pt particles by H_2 that has crossed over the PEM and cathode.

$${Pt_{(*)}}^{z+} + \frac{z}{2}H_{2(g)} \rightarrow Pt_{(s)} + z{H_{(*)}}^{+} \quad (4)$$

The mechanism described above is a representational hypothesis based on the phenomenon of Pt redistribution during the aging processes.

Concerning the direction and degree of the Pt particle migration and redistribution, the result presented in current literature is not always consistent. For example, when conducting a square-wave potential experiment between 0.87 and 1.2 V vs. RHE, Bi and Fuller [60] found that Pt migrated into the PEM near the cathode. However, Ferreira et al. [49] and More et al. [48] observed Pt enrichment at the cathode/membrane interface, while Xie et al. [29] and Guilminot et al. [45] observed Pt enrichment at the anode/membrane interface. The main reason for the diversity of results is that Pt migration and redistribution is a complex process affected by many factors such as potential, operating time, potential cycle numbers, cell operating conditions, gas permeability of the membrane, and other component conditions. Therefore, more detailed explanations of the Pt redistribution and its degradation effect on cell performance are needed for a more profound understanding of the specific characteristics of Pt catalyst behavior during operation.

3.1.3. Active sites contamination

Another likely cause of severe degradation of the CL in PEM fuel cells is contamination. In general, contamination can be categorized into two groups based on the sources: the first source includes gas contaminates from the fuel and the air (such as CH_4, CO, CO_2, H_2S, NH_3, NO, NO_2, SO_2, SO_3, and O_3); and the second source includes system-derived contaminants, such as trace amounts of metallic

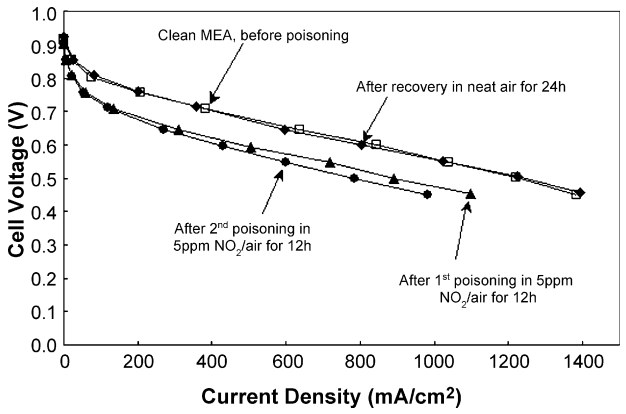

Fig. 4. Polarization for steady-state performance showing the effects of 5 ppm NO_2/air (Adapted from Ref. [64] with permission.)

ions or silicon from system components (e.g., bipolar metal plates, membranes, and sealing gaskets) [61]. Depending on effective time, poison dose, and the reversibility of the poison effect, different contaminants exhibit different poisonous characteristics on Pt catalysts in PEM fuel cells.

In literature, the most extensively investigated contaminant is CO. CO can adsorb preferentially on the Pt catalytic active sites and thus block access of H_2 to these sites and decrease the activity of the catalyst. Even trace amounts of these impurities from the reactant gas are likely to reduce fuel cell performance due to kinetic losses of the anode, especially during long-term operation [62].

Some sulfur-containing species are also contaminants that can create irreversible effects on the catalyst and have a strong negative impact on cell performance. For example, Garzon et al. [63] observed that the cell performance had almost completely deteriorated after 21 h of operation at a constant voltage of 0.5 V when 1 ppm H_2S was added in the anode hydrogen feed. CV results showed the presence of sulfur species chemisorbed onto the Pt surface. Mohtadi et al. [64] also detected two sulfur species formed on the Pt cathode by CV after exposure to either SO_2 or H_2S. They were identified as strongly and weakly adsorbed sulfur on Pt.

For some contaminants in the feeding gas, such as NO_2, the negative influence on the fuel cell is reversible. The experimental results of Mohtadi et al. [64] showed that fuel cell performance decreases as a result of NO_2 impurities could be recovered by applying clean air after exposure to the contaminated air. CV spectra of the clean and poisoned MEAs indicated that the poisoning mechanism of NO_2 is not catalyst related. Fig. 4 shows the recovery of the cell after NO_2 poisoning. The contamination mechanism could be an ionomer effect and/or a catalyst–ionomer interface effect due to the formation of NH_4 from NO_2.

Other impurities such as Cl^- contained anions are also possible contaminants that can induce negative effects on Pt catalyst and performance of PEM fuel cells. These contaminants might come from the preparation of the catalyst or from the feed-stream of the fuel cell. Schmidt et al. [65] investigated that the ORR activity of Pt catalysts with different anions decreased in the order of $ClO_4^- > HSO_4^- > Cl^-$. This order is consistent with the increasing adsorption bond strength of the anions. By using TEM, CV, and EPMA, Matsuoka et al. [66] also proved that the Cl^- caused performance changes. The authors described the poison mechanism of Cl^- in two steps: (1) Cl^- promotes the dissolution of Pt and produces Pt ions ($[PtCl_4]^{2-}$ or $[PtCl_6]^{2-}$) in the inlet-side of the cathode, and (2) the Pt produced ions are reduced into metal Pt by the crossover H_2 and deposited in the PEM to form a Pt band.

3.2. Mitigation strategies

3.2.1. Platinum catalyst alloyed or modified by other metals

To improve the durability of PEM fuel cell catalysts for long-term operation, extensive research has been conducted on Pt catalyst alloyed or modified by other metals that are designed to avoid serious activity losses that result from Pt growing and Pt migration. This strategy also helps lower the Pt loading and the cost of the fuel cell. For instance, PtRu/C [67] and PtSn/C [68] catalysts have been well researched and were found to endure the poison of CO contamination well.

The most attractive elements to alloy with Pt are selected from a variety of transition metals. Co, Cr, Fe, Ni and Pd contained Pt alloys have been synthesized using several preparation methods and have been investigated in PEM fuel cells. Tarasevich et al. [69] compared the durability of PtCo/C and Pt/C catalysts by corrosion tests carried out in a 0.5 M H_2SO_4 solution. The temperature of the solution was periodically increased up to 60 °C and the testing was performed in the presence of 10% H_2O_2 or air bubbling. The experimental results showed that the amount of dissolved Pt for PtCo/C (the alloy exists in two phases: Pt_3Co and PtCo) was lower than Pt/C and did not increase with increased exposure to corrosion. However, in this paper no further results were presented besides the results from the purely chemical corrosion test. Other reports [70,71] have also demonstrated that Pt-alloy catalysts containing cobalt show significantly improved durability in potential cycling compared to unalloyed Pt. The durability improvements of the PtCo catalysts are attributed to their special structure (e.g., smaller Pt–Pt bond distance) and surface electronic properties (e.g., inhibiting OH_{ads} formation), which provide more activity sites for fuel cell reactions.

Similar to Pt-based alloy catalysts, modified-Pt catalysts also show potentials in improving the durability of Pt-based catalyst. For example, Koh and Strasser [72] reported a “de-alloying” method to prepare Pt-Cu catalysts with a core-shell nano-particle structure. The result demonstrated that the electrochemical de-alloying of Cu from Pt-Cu bimetallics significantly altered the catalyst surface activities and improved its durability under potential cycling conditions. Chen et al. [73] developed supportless Pt and Pt-Pd nanotubes with high durability and activity for the ORR in PEM fuel cells. The authors associated these excellent properties with the unique combination of dimensions on multiple length scales, which could have the potential to eliminate or alleviate most of the degradation pathways of traditional catalysts.

3.2.2. Potential application of non-platinum catalyst

Although the original purpose of non-Pt catalyst development was to lower the cost of PEM fuel cells, they also have potential benefits to increase the durability of the fuel cells due to their unique catalytic mechanisms. Currently, the most promising non-Pt catalysts are N contained transit metal macrocyclic complexes with such structures as phthalocyanines, porphyrines, and related derivatives. The origin of the electrocatalyst activity of the N-contained non-Pt catalyst was believed to be the N_4-chelates (or N_2-chelates) of transition metals due to the simultaneous presence of metal precursors, active carbon, and a nitrogen source under pyrolysis conditions. Accordingly, the N-contained non-Pt catalysts do not need to conquer the durability issues occurs to the Pt catalysts during long-term operations. The major problem is that these non-Pt catalysts are not mature enough to be applied at the current technical stage, since their performances are quite low compared with that of the Pt-based catalyst. However, many researchers are attempting to improve the quality of the non-Pt catalyst. For example, recently, Lefèvre et al. [74] reported an iron-based (Fe/N/C) catalyst prepared by a novel method with a great activity improvement due to increased active sites. The reported current density of the cathode

made with this catalyst matched the performance of Pt/C catalyst with a loading of 0.4 mg cm^{-2}. It is possible that non-Pt composite materials will make a real breakthrough to lower the cost and improve the performance of fuel cells in the near future.

4. Carbon support degradation

Nano-scaled Pt particles are usually distributed on carbon support materials to obtain a maximum utilization ratio and to decrease the cost of fuel cells. However, under prolonged operation at high temperatures, high water content, low pH, high oxygen concentration, existence of the Pt catalyst and/or high potential, carbon support is prone to degrade both physically and chemically, which is called carbon oxidation (or carbon corrosion). Carbon oxidation weakens the attachment of Pt particles to the carbon surface, and eventually leads to structural collapse and the detachment of Pt particles from the carbon support, resulting in declines of the catalyst active surface area and fuel cell performance. In Sato et al.'s study [75], it was proven that no performance degradation occurred when a Pt-black catalyst was applied as the anode electrode catalyst. Under the same hydrogen starvation operation, however, the Pt/C catalyst based fuel cell experienced severe degradation. Generally, carbon corrodes under three conditions: (1) normal operating potentials, (2) gross fuel starvation at the anode, and (3) partial hydrogen coverage at the anode.

4.1. Carbon corrosion mechanisms

Carbon corrosion may occur as a chemical or an electrochemical process. More specifically, carbon oxidation takes place along two pathways that are believed to proceed by electron transfer, followed by hydrolysis and CO_2 production: (1) incomplete oxidation leading to the formation of surface groups (Eqs. (5) and (6); and (2) complete oxidation leading to gaseous carbon dioxide (Eq. (7)) [76].

$$C_s \rightarrow C_s^+ + e^- \quad (5)$$

$$C_s^+ + \tfrac{1}{2}H_2O \rightarrow C_sO + H^+ \quad (6)$$

$$C_sO + H_2O \rightarrow CO_2(g) + 2H^+ + 2e^- \quad (7)$$

The subscript "s" denotes the surface species.

For instance, according to Baumgartner et al.'s report [77], CO and CO_2 were detected from both the anode and cathode exhausts during degradation test. Carbon corrosion is sensitive to many factors such as potential, carbon surface area, and relative humidity within the fuel cell. Among these factors, potential is the most aggressive. Kangasniemi et al. [78] showed evidence of surface oxidation occurring on Vulcan carbon when potentials were greater than 0.8 V at 65 °C and greater than 1.0 V at room temperature. Therefore, carbon corrosion on the cathode is more serious than that on the anode during normal steady-state operation. This was proven by an observed thickness decrease after long periods of operation, especially at high potentials such as OCV and idle conditions [44,45,57].

When undergoing unprotected and frequent startup/shutdown of a fuel cell, local cathode potentials can reach up to 1.5 V due to non-uniform distribution of fuel to the anode [11,79], accelerating carbon corrosion. Moreover, carbon is prone to be oxidized at lower potentials in the presence of Pt. Roen et al. [80] measured the CO_2 emissions of pure carbon and Pt-catalyzed carbon by on-line mass spectrometry. Their results showed that the presence of Pt in the electrode layer could accelerate the carbon corrosion rate at low temperatures. Also, the magnitude of the CO_2 peaks with respect to cell potential depended on the Pt content in the electrode as well.

4.1.1. Gross fuel starvation

When the fuel is insufficient to provide the expected current for the PEM fuel cell (called fuel starvation), the potential value of the anode increases. With anode potential increasing, the cell potential can decrease to a value substantially below normal and even drive the cell into reverse operation, where the anode potential is higher than the cathode potential. Once the potential of the anode rises to above 0.207 V or further to over 1.23 V with the fuel consumption, water electrolysis and carbon oxidation at the anode will occur to provide the required protons and electrons for the ORR at the cathode [81]:

$$C + 2H_2O = CO_2 + 4H^+ + 4e^- \qquad E_{298\,K} = +0.207\,V \text{ vs. RHE} \quad (8)$$

$$H_2O = \tfrac{1}{2}O_2 + 2H^+ + 2e^- \quad E_{298\,K} = +1.229\,V \text{ vs. RHE} \quad (9)$$

These reactions can be observed when the fuel cell experiences bad flow distribution, gas blockages, or sudden current changes due to heavy load under transient conditions. Using TEM, EDX, and electrochemical methods, Taniguchi et al. [82] characterized electrocatalyst degradation caused by fuel starvation and found severe surface area losses of the electrocatalyst, as well as a drop in cell performance due to carbon support corrosion after cell reversal. Electrochemical surface area decreased after only 1 s of operation under cell reversal conditions.

The effects of cell reversal caused by air starvation were much smaller than that of fuel starvation [83]. However, the ECSA still decreased by 46% after 120 min of cell reversal caused by air starvation, which was much greater than under normal operation conditions.

4.1.2. Corrosion due to air/fuel boundary

Carbon corrosion can also arise from a non-uniform distribution of fuel on the anode side (partial hydrogen coverage) and from crossover of reactant gas through the membrane. Both startup and shutdown, as well as local fuel starvations, can cause this type of carbon corrosion. Tang et al. [84] investigated this type of carbon corrosion using both single-cell and dual-cell configurations and explained the results with the air/hydrogen boundary mechanism. Fig. 5 shows a schematic illustration of reactions when an air/fuel boundary is formed at the anode. When oxygen is present on the anode side, the ORR will occur in this area. The carbon oxidation reaction (8) and water electrolysis reaction (9) will occur on the corresponding cathode side. According to the experimental results, the most pronounced corrosion damage was found within the first 30 cycles, when air and fuel were alternately fed to the anode. The cathode ECSA loss was as high as 70% after 80 such cycles.

Raiser et al. [85] credited similar carbon decay to the anode electrode being partially filled with hydrogen. They modeled this corrosion phenomenon using simplified mathematical approaches, thereby obtaining an electrolyte potential profile. The authors con-

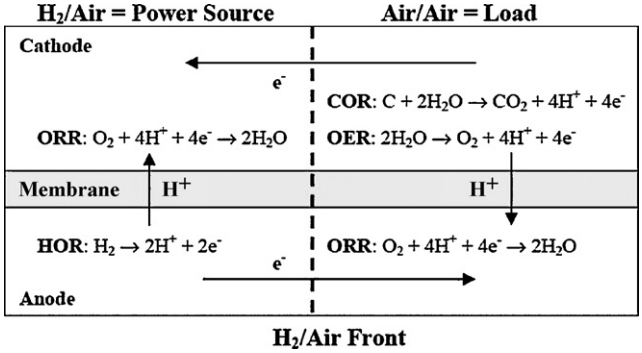

Fig. 5. The schematic of the fuel/air boundary mechanism and the involved electrochemical reactions (From Ref. [89] with permission.)

cluded that oxygen crossover from the cathode side was sufficient to cause a reverse-current condition and correspondingly cause permanent damage to the cathode of PEM fuel cells. Meyers and Darling [86] developed a model to explain the reverse-current mechanism and suggested that the carbon corrosion rate induced by local fuel starvation can be mitigated by careful system control and design. Also, based on the partial hydrogen coverage model, Fuller and Gray [7] explained that higher cell potential, lower conductivity of the ionomer, and greater permeability of oxygen through the separator are all conditions under which the susceptibility to carbon corrosion will be greater.

Air/hydrogen boundary mechanism for carbon corrosion can also explain why the cathode layer after startup and shutdown aging is normally thinner than the anode layer [84,85,87]. Also, the sharp voltage change might cause some damage to Nafion®, and the combination of these effects could entirely explain MEA degradation during ASTs involving startup/shutdown cycles [86,88]. To summarize, carbon corrosion has been identified as a crucial degradation mechanism, especially for automotive applications due to the frequent startups and shutdowns.

4.2. Mitigation strategies

4.2.1. Novel carbon supports

One possible mitigation strategy to reduce the negative influence of carbon oxidation on fuel cell performance is to use more stable materials as catalyst supports, e.g., carbon supports with a greater graphitization degree. Yu et al. [89] proved that graphitized carbon supported catalysts showed higher resistance to carbon corrosion than conventional Pt/C catalysts by a factor of 35 at a point where 5% weight loss had occurred. After 1000 startup/shutdown cycles, the graphitized carbon MEA yielded a lower degradation rate by a factor of 5 than that of a conventional carbon MEA without any system mitigation methods applied. Similarly, Owejan et al. [90] investigated the implementation of graphitized carbon in the microporous layer (MPL). Compared to conventional carbon fabricated MPLs, they observed a 25% improvement in the startup/shutdown degradation rate at 1.2A cm^{-2}.

Carbon nanotubes or carbon nanofibers have recently been proposed as promising support materials for fuel cell catalysts due to their unique characteristics such as high aspect ratio, high electron conductivity, specific interaction with Pt catalyst, and enhanced mass transport capability. Many groups have investigated their durability capabilities to replace normal carbon black in PEM fuel cells [91–93]. For example, Wang et al. [79] reported that multiwalled carbon nanotubes were electrochemically more stable than Vulcan XC-72. They experienced less surface oxide formation and 30% lower corrosion current under 0.9 V in a 0.5 M H_2SO_4 solution. This led to lower losses in Pt surface area and oxygen reduction reaction activity in PEM fuel cell catalyst supports.

More recently, carbon aerogel [94,95] and xerogel [96] have also shown potential as an alternative catalyst support in PEM fuel cells. They have a controllable network structure, which is believed to be able to improve the stability and provide good contact with the ionically conductive polymer electrolytes in the CL.

4.2.2. Potential application of non-carbon supports

In spite of high carbon corrosion resistance, graphitized carbon has a lower surface area. Also, high dispersion of noble metals inside tubular carbon fibers is rather difficult because of the diameter-to-length ratio of a single nanotube [97]. Furthermore, carbon degradation will not be mitigated under severe conditions even when highly graphitized carbon is used, since graphitization can only slow down the kinetics of the carbon oxidation reaction, but will not change the fundamental oxidation mechanisms [103]. Therefore, further investigation for other alternative support materials is required. To date, some novel materials such as substoichiometric titanium oxide [98], tungsten carbide [99], tungsten oxide [100], indium tin oxide [101], and sulfonated zirconium oxide [102] have been investigated to improve the support durability. All these materials showed greater stability than conventional carbon supports under different accelerated durability tests. However, both of the synthesis techniques and required properties of these novel supports (such as surface area, conductivity, interaction with Pt, and dispersion ability) need to be optimized in further studies.

4.2.3. System strategies

System mitigation strategies can also help to improve the durability of the support material, especially when alternative supports cannot offer adequate protection from carbon corrosion if the electrode is exposed to high potentials. For example, UTC Power (United Technologies Corp.) has proposed some system mitigation strategies, such as (1) minimizing the time that the adverse conditions exist, (2) controlling the potentials during startups and shutdowns by using external loads, and (3) minimizing the number of adverse cycles that occur in a given application [104]. Specific examples of the procedure can also be found in some patents [105–108].

5. Ionomer degradation and interfacial degradation

Typically, carbon supported Pt or modified/alloyed Pt catalysts are partially embedded in a proton conducting polymeric ionomer, such as a recast Nafion ionomer, which mediates proton migration as well as water transport inside its pore system. Fig. 6 shows a model of a Pt/ionomer/C microstructure that creates the critical 3-phase interface. Except the Pt catalyst and the carbon support, Nafion ionomer also plays an important role in the CL to influence the structure and performance. The distribution of the ionomer, as well as its content in the CL, can directly impact the ionic/electronic conductivity of the CL [109,110]. Both chemical/physical degradation and dissolution of the recast ionomer in CL could lead to a decrease in ionic/electronic conductivity and mass transport ability of the MEA.

Another aspect concerning the ionic/electronic conductivity and mass transport on a macroscopic scale is the interfacial components alternation of CL/PEM and CL/GDL during the aging process, which is also a source of performance degradation of PEM fuel cell, especially under extreme conditions.

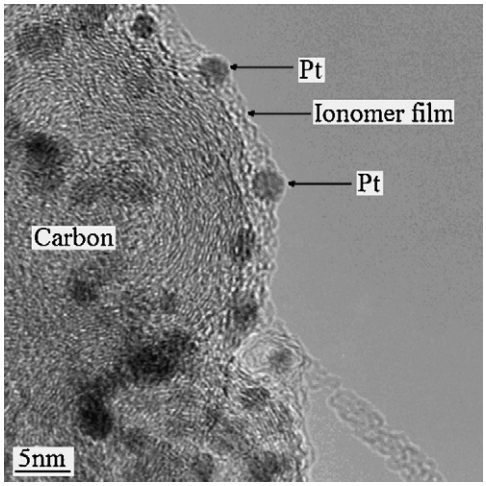

Fig. 6. A TEM image showing model structure of Pt/ionomer/C microstructure that creates the critical 3-phase interfaces (From Ref. [48] with permission.)

5.1. Ionomer degradation

It is known that the hydrogen peroxide, OH radicals or other contaminants produced during the fuel cell reaction are all potential species that damage the functionality and integrity of the Nafion membrane by attacking the perfluorosulfonic acid (PFSA). The same damage could happen to the recast Nafion ionomer employed in the CL during the aging process. The major difference of the ionomer degradation in the CL from that in the PEM is two-sided. On the one hand, the Nafion ionomer in the CL is located adjacent to the fuel cell reaction active sites. Nafion ionomer degradation at these locations can accordingly be slower than that in the membrane, since some of the radical species might be scavenged by the Pt catalyst [111]. On the other hand, the recast Nafion ionomer in the CL is exposed to more water (from both product water generation and inlet water flow) and intermediates under operating conditions. Therefore, the dissolution and chemical degradation of the recast ionomer in the CL might be more severe than that in the PEM [44]. However, there is no sufficient data so far to determine which of the two aspects is weightier than the other. More work is still needed to quantitatively determine the ionomer degradation in both the CL and the PEM.Many research groups addressed that the ionomer degradation/loss might be one of the critical factors that lead to the reduced performance of the CL after long-term operation or AST. Generally, the actual Nafion ionomer network within the CL was not as easily distinguished/imaged as Pt and carbon support, when using traditional morphology characterization methods. However, some research groups have made a remarkable progress in confirming the Nafion ionomer degradation in CLs recently.Using cell impedance trends, Xie et al. [29] revealed the degradation of the recast ionomer network in the CL after 500 h of operation under high humidity and constant current. In another quantitative analysis performed with XPS, Zhang et al. [110] detected the CL ionomer degradation (or decrease in concentration) after 300 h of fuel cell operation. According to their report, the CL surface concentration of fluorine reduced from 50.1% to 38.9%, consistent with a decrease of CF_3 and CF_2 species and an increase in oxidized forms of carbon, which undoubtedly was a proof for the Nafion ionomer change. And with EIS, Hou et al. [112] measured the ionic resistances of the CL at different current densities after the PEM fuel cell suffered from sub-freezing condition. The authors explained that the change of the ionic resistance profile, which was not even across the entire CL, was induced by the ice formation when the temperature reached −10 °C. Since the ionic resistance of the cell has been shown to depend primarily on the CL recast ionomer [113,114], it is reasonable to conclude that ionomer network degradation is the main reason for the CL degradation in this case. Based on a microstructure reconstruction simulation using statistical information from experimental images of the CLs, Rong et al. [115] also suggested that the competition between the delamination energy accumulated on the interface between Nafion ionomer and the Pt/C agglomerate and the plasticity energy accumulated in the Nafion ionomer plays a key role in microstructure changes during PEM fuel cell aging. However, the understanding of ionomer degradation inside the CL is not thorough enough corresponding to its high importance. Further efforts on the degradation mechanisms of the Nafion recast ionomer on both the anode and the cathode CL, as well as more advanced testing methods and mitigation methods, are urgently required.

5.2. Interfacial degradation

As the microstructural changes inside the CL accumulate with time, they will undoubtedly lead to a decrease in connection between different solid phases and even mechanical damage to the MEA. As mentioned by Kundu et al. [116], these delaminations could cause increased resistance, loss of apparent catalytic activity, and development of flooded areas and pinholes, etc. Guilminot et al. [57] reported an obvious separation and cracks at aged cathode/membrane interfaces during a 529-h constant-power test ($0.12\ W\ cm^{-2}$). They proved that delaminations and cracks between the CL and the PEM or GDL occur more easily due to relative humidity and temperature changes during load cycles. These interfacial degradations have been considered unrecoverable and permanent compared with the recoverable and temporary changes due to water content changes [117,118].

The most serious interfacial degradation for PEM fuel cells occurs during subzero startups and freeze/thaw cycling. During cold startups in subzero environments, water produced in the CL may freeze instantaneously in the pore systems, covering the electrochemical active sites, hence reducing reaction capability and damaging the interface structure [119,120]. Yang et al. [121] characterized the cross-sectional samples of the aged MEAs after 110 cold startup cycles. By using TEM and XRD, they confirmed that interfacial delaminations between the CL and PEM and the cathode CL pore collapse were among the degradation mechanisms resulting from cold startups. They also explained that the damage degree to the MEA was related to the settling startup current density. CL delamination from both the PEM and the GDL was also observed by Yan et al. [122] during cold startup studies under a wide range of operating conditions. Results showed that when the cell cathode temperature fell below −5 °C during the operation, irreversible cell performance losses were found due to the internal component damages.

Similarly, under frequent freeze/thaw cycles, a shear force induced by phase transition between water and ice will cause uneven mechanical stress for different components, resulting in interfacial delaminations and damages [123,124,125]. For instance, Kim et al. [126] reported interfacial delamination between the CL and GDL after 100 freeze/thaw cycles from −40 °C to 70 °C. These delaminations caused by the ice formation will in turn significantly deform the GDL.

Since ice formation is the main reason for structural and performance degradation during exposure to sub-zero temperatures, attention has been paid to minimize the negative effects brought by water. Currently, the most effective way to mitigate interfacial degradation under subzero conditions is to control the water content in the MEA [121,124,127].

6. Summary

In general, CL degradation can occur from each component (catalyst, support, and ionomer) and the interfaces between them. Both the microstructural/macrostructural changes and the material losses in the CL can affect fuel cell performance and durability. All of these factors result in either a change of catalyst activity or a loss of ionic/electronic contact compared with the original system. Typical CL degradation modes and corresponding investigation methods discussed in Sections 2–5 are summarized in Table 2, including degradations originated from catalyst material, carbon support, Nafion ionomer in the CL, and interfacial changes. Principal causes and general experimental protocols under both steady state and accelerated conditions are also listed to clearly demonstrate the investigating methods for different CL degradation mechanisms. Correspondingly, Table 3 lists current and potential mitigation strategies for different degradation modes in the CL. Some useful examples, including novel materials and system modifications, as well as the advantages of some strategies are also summed up. It is clearly shown that both the material exploration and system modification strategies are important to solve the current degradation problems in the CL of PEM fuel cells.

Table 2
Summary of PEM fuel cell catalyst degradation/failure modes and experimental protocols.

Degradation mode	Principle causes	General methods	Experimental protocols	References
Pt degradation	Pt particle growth	Potential cycling (scanning, square wave cycling, or triangular wave cycling)	Potential cycling from 0.6 to 1.2 V (vs. RHE) at 300 mV s^{-1} for 10,000 cycles	[27]
			Potential cycling between 0 and 1.3 V (vs. RHE) at 50 mV s^{-1} for 1000 times in Ar purged 0.5 M H_2SO_4 solution	[73]
			Potential cycling between three different ranges: 0.1–0.7 V, 0.1–1.0 V, and 0.1–1.2 V	[48]
			Potential cycling between 0.4 and 1.4 V at 1.0 V s^{-1} for 4 h	[31]
			Potential cycling from 0.6 to 1.2 V at 20 mV s^{-1} for 1000 times and holding at 1.2 V for 24 h in He feed in 0.5 M H_2SO_4 at 75 °C and in 130 °C fuel cell	[28]
			Potential cycling from 0.5 to 1.5 V with different wave profiles	[51]
		Potential holding	Potential holding at 1.4 V and 1.2 V	[43]
			Potential holding at 1.2, 1.0 V and 0.8, 0.6 V in oxygen and nitrogen atmosphere, respectively	[32]
			Potential holding at 0.90 V for 480 h	[40]
		Long time operation under different conditions	Constant-current (1.07 A cm^{-2}) mode operation at 80 °C under high humidity for 1000 h	[29]
			Constant-power operation at 0.12 W cm^{-2} for 529 h	[57]
			Dynamic load cycling to simulate the drive cycles	[53]
	Pt loss or migration	Potential cycling	Square wave potential cycling for 7000 cycles between 0.87 and 1.2 V (vs. RHE) for 30 s at each potential	[60]
			Potential cycling between three different ranges: 0.1–0.7, 0.1–1.0, and 0.1–1.2 V for 1500 cycles	[48]
		Potential holding (including OCV holding)	Potential holding of 1.0 V under air or N_2 for the cathode and pure H_2 for the anode	[58]
			2000 h of open-circuit operation under H_2/air supply conditions	[49]
			Constant-power operation at 0.12 W cm^{-2} for 529 h	[57]
			Constant-current (1.07 A cm^{-2}) mode operation at 80 °C under high humidity for 1000 h	[29]
	Contamination	Contamination from the air	Constant voltage operation at 0.68–0.70 V with exposure to SO_2, NO_2, and H_2S in the cathode air feed	[64]
		Contamination from the fuel	Constant voltage operation at 0.5 V with exposure to a 1 ppm H_2S in the anode hydrogen feed for 21 h	[63]
		Anion contamination	Different anion species supplied with cathode gas for 50 h at a current density of 0.3 A cm^{-2}	[66]
Carbon support degradation	Carbon corrosion	Potential cycling to high potentials	Potential step cycling of 1.4 V, 150 s to 0.85 V, 30 s and 1.4 V, 150 s to 0.6 V, 30 s	[43]
		Potential holding at high potential	Potential holding of 1.4 and 1.2 V	[43]
			Potential holding at 1.2, 1.0 V and 0.8, 0.6 V in oxygen and nitrogen atmosphere, respectively	[32]
			Potential holding at 0.90 V for 480 h	[40]
		Long time operation	Constant-power operation at 0.12 W cm^{-2} for 529 h	[57]
		Cell reversal caused by fuel/air starvation	Cell reversal experiment caused by fuel starvation	[82]
			Cell reversal experiment caused by air starvation	[83]
			Fuel starvation simulated in a 3-cell stack	[75]
			Fuel starvation experiment	[77]
		Startup/shutdown cycling	Simulate startup and shutdown operations with a single cell	[88]
Ionomer degradation	Ionomer degradation	Long time operation	Constant current mode operation under high humidity	[44]
Interfacial degradation	Interfacial change between CL/PEM or CL/GDL	Freeze/thaw cycling	Freeze/thaw cycles between −40 °C and 70 °C on PEM fuel cell in water-submerged conditions	[126]
			Freeze/thaw cycles on fully humidified fuel cells to various sub-freezing temperatures	[125]
		Cold-startup cycling	Cold startup at −30 °C at different current densities with a single cell: 100, 300 mA cm^{-2}, −20 °C at 500 mA cm^{-2}	[121]
			Cold startup at −40 °C with a 6-cell stack with constant gas flow rates	[122]
		Long time operation	Constant-power operation at 0.12 W cm^{-2} for 529 h	[57]

Table 3
Summary of mitigation strategies for different degradation modes in PEM fuel cell catalyst layers.

Degradation mode	Mitigation strategies	Comments	Examples	References
Pt degradation	Modified or alloyed Pt catalyst	Helps lower the Pt loading and the cost of fuel cell	PtRu/C; PtSn/C; PtCo/C; etc.	[13,14,67–71]
	Non-Pt catalyst	Unique catalytic mechanisms and low price	Non-noble metals; N contained transit metal macrocyclic complexes; etc.	[15,16]
Carbon degradation	Novel carbon support	Unique characteristics and controllable structure	Carbon nanofibers and nanotubes; carbon aerogel and xerogel; etc.	[79,91–96]
	Non-carbon support	Excellent stability	Substoichiometric titanium oxide; tungsten carbide; tungsten oxide; indium tin oxide; etc.	[98–102]
	System strategies	Avoid the severe conditions that result in carbon corrosion	Minimizing the adverse conditions and avoiding high potential using external loads; etc.	[104–108]
Interfacial degradation due to subzero temperatures	Water removal and system modification	Avoid ice formation under subzero conditions	Gas purging; thermal insulation; etc.	[121,124,127]

7. Concluding remarks

CL degradation during long-term operation under universal conditions is a complex process that includes many mechanisms that occur in parallel. This review provides a structural understanding of the significant factors affecting CL degradation including: Pt catalyst ripening, electrocatalyst loss or redistribution, carbon corrosion, electrolyte (Nafion ionomer) degradation, and interfacial degradation.

Studies of degradation mechanisms of CL under long-term operation are equally as important as studies of simulated accelerated stress conditions. Extensive effort has been put into this study for half-cells, single cells, and stacks. It is worth noting that each system level of research is valuable and irreplaceable because of its own characteristics. Therefore, conclusions must be drawn cautiously based on a comprehensive research that considers both the real fuel cell operation and the effects of interactions between different materials.

Currently, improvements to traditional CL materials are important to the commercialization of PEM fuel cells in the near future. At the same time, research on novel materials is also a key aspect in dealing with issues related to CL degradation. Attractive materials that are in development include: Pt catalysts with highly ordered and optimized structure, non-platinum catalysts, and non-carbon supports with excellent characteristics. Also, more attention should be paid to ionomer and interfacial degradation to investigate fundamental mechanisms with respect to their significant influences on the CL degradation.

Acknowledgments

The authors acknowledge the NRC-Helmholtz Joint Research Program, the NRC-MOST Joint Research Program, and BCIC's ICSD Program for financial support.

References

[1] J. Wu, X.Z. Yuan, J.J. Martin, H. Wang, J. Zhang, J. Shen, S. Wu, W. Mérida, J. Power Sources 184 (2008) 104–119.
[2] V.A. Sethuraman, J.W. Weidner, A.T. Haug, L.V. Protsailo, J. Electrochem. Soc. 155 (2008) B119–B124.
[3] W. Liu, M. Crum, ECS Trans. 3 (2006) 531–540.
[4] A.B. LaConti, H. Liu, C. Mittelsteadt, R.C. McDonald, ECS Trans. 1 (2006) 199–219.
[5] R.L. Borup, J.R. Davey, F.H. Garzon, D.L. Wood, P.M. Welch, K. More, ECS Trans. 3 (2006) 879–886.
[6] S. Mitsushima, S. Kawahara, K. Ota, N. Kamiya, J. Electrochem. Soc. 154 (2007) B153–B158.
[7] T.F. Fuller, G. Gray, ECS Trans. 1 (2006) 345–353.
[8] A.A. Franco, M. Gerard, J. Electrochem. Soc. 155 (2008) B367–B384.
[9] D.L. Wood, J.R. Davey, P. Atanassov, R.L. Borup, ECS Trans. 3 (2006) 753–763.
[10] M. Oszcipok, D. Riemann, U. Kronenwett, M. Kreideweis, M. Zedda, J. Power Sources 145 (2005) 407–415.
[11] P.P. Wells, Y. Qian, C.R. King, R.J.K. Wiltshire, E.M. Crabb, Faraday Discuss. 138 (2008) 273–285.
[12] P. Mani, R. Srivastava, P. Strasser, J. Phys. Chem. C 112 (2008) 2770–2778.
[13] Y. Qian, W. Wen, P.A. Adcock, Z. Jiang, N. Hakim, M.S. Saha, S. Mukerjee, J. Phys. Chem. C 112 (2008) 1146–1157.
[14] M.C. Denis, M. Lefevre, D. Guay, J.P. Dodelet, Electrochim. Acta 53 (2008) 5142–5154.
[15] S. Izhar, M. Yoshida, M. Nagai, Electrochim. Acta 54 (2009) 1255–1262.
[16] F. Charreteur, S. Ruggeri, F. Jaouen, J.P. Dodelet, Electrochim. Acta 53 (2008) 6881–6889.
[17] X. Yu, S. Ye, J. Power Sources 172 (2007) 145–154.
[18] H.A. Gasteiger, S.S. Kocha, B. Sompalli, F.T. Wagner, Appl. Catal. B: Environ. 56 (2005) 9–35.
[19] E. Antolini, J.R.C. Salgado, E.R. Gonzalez, J. Power Sources 160 (2006) 957–968.
[20] Y. Shao, G. Yin, Y. Gao, J. Power Sources 171 (2007) 558–566.
[21] R. Borup, J. Meyers, B. Pivovar, Y. Seung Kim, R. Mukundan, N. Garland, D. Myers, M. Wilson, F. Garzon, D. Wood, P. Zelenay, K. More, K. Stroh, T. Zawodzinski, J. Boncella, J.E. McGrath, M. Inaba, K. Miyatake, M. Hori, K. Ota, Z. Ogumi, S. Miyata, A. Nishikata, Z. Siroma, Y. Uchimoto, K. Yasuda, K. Kimijima, N. Iwashita, Chem. Rev. 107 (2007) 3904–3951.
[22] P. Rama, R. Chen, J. Andrews, Proc. IMechE Part A: J. Power Energy 222 (2008) 421–441.
[23] W. Schmittinger, A. Vahidi, J. Power Sources 180 (2008) 1–14.
[24] S. Zhang, X. Yuan, H. Wang, W. Mérida, H. Zhu, J. Shen, S. Wu, J. Zhang, Int. J. Hydrogen Energy 34 (2009) 388–404.
[25] Z.-B. Wang, P.-J. Zuo, X.-P. Wang, J. Lou, B.-Q. Yang, G.-P. Yin, J. Power Sources 184 (2008) 245–250.
[26] M. Uchimura, S. Kocha, ECS Trans. 11 (2007) 1215–1226.
[27] H. Yoshida, T. Kinumoto, Y. Iriyama, Y. Uchimoto, Z. Ogumi, ECS Trans. 11 (2007) 1321–1329.
[28] A.S. Aricò, A. Stassi, E. Modica, R. Ornelas, I. Gatto, E. Passalacqua, V. Antonucci, ECS Trans. 3 (2006) 765–774.
[29] J. Xie, D.L. Wood III, K.L. More, P. Atanassov, R.L. Borup, J. Electrochem. Soc. 152 (2005) A1011–A1020.
[30] W. Bi, T.F. Fuller, J. Power Sources 178 (2008) 188–196.
[31] K.J.J. Mayrhofer, J.C. Meier, S.J. Ashton, G.K.H. Wiberg, F. Kraus, M. Hanzlik, M. Arenz, Electrochem. Commun. 10 (2008) 1144–1147.
[32] Z. Siroma, K. Ishii, K. Yasuda, M. Inaba, A. Tasaka, J. Power Sources 171 (2007) 524–529.
[33] D.A. Bussian, J.R. O'Dea, H. Metiu, S.K. Buratto, Nano Lett. 7 (2007) 227–232.
[34] M. Inaba, H. Ysamada, J. Tokunaga, K. Matsuzawa, A. Hatanaka, A. Tasada, ECS Trans. 1 (2006) 315–322.
[35] F.H. Garzon, S.H. Lau, J.R. Davey, R.L. Borup, ECS Trans. 11 (2007) 1139–1150.
[36] S.H. Lau, W.K.S. Chiu, F. Garzon, H. Chang, A. Tkachuk, M. Feser, W. Yun, J. Phys: Conf. Ser. 152 (2009) (art. no. 012059).
[37] H. Yamada, D. Shimoda, K. Matsuzawa, A. Tasaka, M. Inaba, ECS Trans. 11 (2007) 325–334.
[38] Z. Luo, D. Li, H. Tang, M. Pan, R. Ruan, Int. J. Hydrogen Energy 31 (2006) 1831–1837.
[39] A.S. Aricò, A. Stassi, E. Modica, R. Ornelas, I. Gatto, E. Passalacqua, V. Antonucci, J. Power Sources 178 (2008) 525–536.
[40] T. Yoda, H. Uchida, M. Watanabe, Electrochim. Acta 52 (2007) 5997–6005.
[41] S.Y. Cha, W.M. Lee, J. Electrochem. Soc. 146 (1999) 4055–4060.
[42] J. Wu, X.Z. Yuan, H. Wang, M. Blanco, J.J. Martin, J. Zhang, Int. J. Hydrogen Energy 33 (2008) 1735–1746.
[43] Y. Shao, R. Kou, J. Wang, V.V. Viswanathan, J.H. Kwak, J. Liu, Y. Wang, Y. Lin, J. Power Sources 185 (2008) 280–286.
[44] J. Xie, D.L. Wood III, D.M. Wayne, T.A. Zawodzinski, P. Atanassov, R.L. Borup, J. Electrochem. Soc. 152 (2005) A104–A113.
[45] E. Guilminot, A. Corcella, F. Charlot, F. Maillard, M. Chatenet, J. Electrochem. Soc. 154 (2007) B96–B105.

[46] M. Pourbaix, Altas of Electrochemical Equilibrium in Aqueous Solutions, Pergamon Press, New York, 1966.
[47] R. Dingreville, J. Qu, M. Cherkaoui, J. Mech. Phys. Solids 53 (2005) 1827–1854.
[48] K.L. More, R. Borup, K.S. Reeves, ECS Trans. 3 (2006) 717–733.
[49] P.J. Ferreira, G.J. la O', Y. Shao-Horn, D. Morgan, R. Makharia, S. Kocha, H.A. Gasteiger, J. Electrochem. Soc. 152 (2005) A2256–A2271.
[50] A.V. Virkar, Y. Zhou, J. Electrochem. Soc. 154 (2007) B540–B547.
[51] S. Kawahara, S. Mitsushima, K.-I. Ota, N. Kamiya, ECS Trans. 3 (2006) 625–631.
[52] X.P. Wang, R. Kumar, D.J. Myers, Electrochem. Solid-state Lett. 9 (2006) A225–A227.
[53] R.L. Borup, J.R. Davey, F.H. Garzon, D.L. Wood, M.A. Inbody, J. Power Sources 163 (2006) 76–81.
[54] M. Cai, M.S. Ruthkosky, B. Merzougui, J. Power Sources 160 (2006) 977–986.
[55] H. Xu, R. Kunz, J.M. Fenton, Electrochem. Solid-state Lett. 10 (2007) B1–B5.
[56] S.C. Ball, S.L. Hudson, J.H. Leung, A.E. Russell, D. Thompsett, B.R.C. Theobald, ECS Trans. 11 (2007) 1247–1257.
[57] E. Guilminot, A. Corcella, M. Chatenet, F. Maillard, F. Charlot, G. Berthomé, C. Iojoiu, J.-Y. Sanchez, E. Rossinot, E. Clauded, J. Electrochem. Soc. 154 (2007) B1106–B1114.
[58] T. Akita, A. Taniguchi, J. Maekawa, Z. Siroma, K. Tanaka, M. Kohyama, K. Yasuda, J. Power Sources 159 (2006) 461–467.
[59] R.M. Darling, J.P. Meyers, J. Electrochem. Soc. 150 (2003) A1523–A1527.
[60] W. Bi, T.F. Fuller, J. Electrochem. Soc. 155 (2008) B215–B221.
[61] X. Cheng, Z. Shi, N. Glass, L. Zhang, J. Zhang, D. Song, Z.-S. Liu, H. Wang, J. Shen, J. Power Sources 165 (2007) 739–756.
[62] O. Yamazaki, Y. Oomori, H. Dhintaku, T. Tabata, ECS Trans. 11 (2007) 287–295.
[63] F.H. Garzon, T. Rockward, I.G. Urdampilleta, E.L. Brosha, F.A. Uribe, ECS Trans. 3 (2006) 695–703.
[64] R. Mohtadi, W.-k. Lee, J.W. Van Zee, J. Power Sources 138 (2004) 216–225.
[65] T.J. Schmidt, U.A. Paulus, H.A. Gasteiger, R.J. Behm, J. Electroanal. Chem. 508 (2001) 41–47.
[66] K. Matsuoka, S. Sakamoto, K. Nakato, A. Hamada, Y. Itoh, J. Power Sources 179 (2008) 560–565.
[67] M.T.M. Koper, T.E. Shubina, R.A. van Santen, J. Phys. Chem. B 106 (2002) 686–692.
[68] E.M. Crabb, R. Marshall, D. Thompsett, J. Electrochem. Soc. 147 (2000) 4440–4447.
[69] M.R. Tarasevich, V.A. Bogdanovskaya, E.N. Loubnin, L.A. Reznikova, Prot. Met. 43 (2007) 689–693.
[70] P. Yu, M. Pemberton, P. Plasse, J. Power Sources 144 (2005) 11–20.
[71] S. Ye, M. Hall, H. Cao, P. He, ECS Trans. 3 (2006) 657–666.
[72] S. Koh, P. Strasser, J. Am. Chem. Soc. 129 (2007) 12624–12625.
[73] Z. Chen, M. Waje, W. Li, Y. Yan, ECS Trans. 11 (2007) 1301–1311.
[74] M. Lefèvre, E. Proietti, F. Jaouen, J.-P. Dodelet, Science 324 (2009) 71–74.
[75] Y. Sato, Z. Wang, Y. Takagi, ECS Trans. 3 (2006) 827–833.
[76] K. Kinoshita, Carbon, Electrochemical and Physicochemical Properties, John Wiley & Sons, New York, 1988.
[77] W.R. Baumgartner, E. Wallnofer, T. Schaffer, J.O. Besenhard, V. Hacker, V. Peinecke, P. Prenninger, ECS Trans. 3 (2006) 811–825.
[78] K.H. Kangasniemi, D.A. Condit, T.D. Jarvi, J. Electrochem. Soc. 151 (2004) E125–E132.
[79] X. Wang, W. Li, Z. Chen, M. Waje, Y. Yan, J. Power Sources 158 (2006) 154–159.
[80] L.M. Roen, C.H. Paik, T.D. Jarvi, Electrochem. Solid-state Lett. 7 (2004) A19–A22.
[81] T.R. Ralph, S. Hudson, D.P. Wilkinson, ECS Trans. 1 (2006) 67–84.
[82] A. Taniguchi, T. Akita, K. Yasuda, Y. Miyazaki, J. Power Sources 130 (2004) 42–49.
[83] A. Taniguchi, T. Akita, K. Yasuda, Y. Miyazaki, Int. J. Hydrogen Energy 33 (2008) 2323–2329.
[84] H. Tang, Z.G. Qi, M. Ramani, J.F. Elter, J. Power Sources 158 (2006) 1306–1312.
[85] C.A. Reiser, L. Bregoli, T.W. Patterson, J.S. Yi, J.D. Yang, M.L. Perry, T.D. Jarvi, Electrochem. Solid-state Lett. 8 (2005) A273–A276.
[86] J.P. Meyers, R.M. Darling, J. Electrochem. Soc. 153 (2006) A1432–A1442.
[87] T. Patterson, R. Darling, Electrochem. Solid-state Lett. 9 (2006) A183–A185.
[88] Y. Takagi, Y. Takakuwa, ECS Trans. 3 (2006) 855–860.
[89] P.T. Yu, W. Gu, R. Makharia, F.T. Wagner, H.A. Gasteiger, ECS Trans. 3 (2006) 797–809.
[90] J.E. Owejan, P.T. Yu, R. Makharia, ECS Trans. 11 (2007) 1049–1057.
[91] Y. Shao, G. Yin, Y. Gao, P. Shi, J. Electrochem. Soc. 153 (2006) A1093–A1097.
[92] M.M. Waje, W. Li, Z. Chen, Y. Yan, ECS Trans. 3 (2006) 677–683.
[93] K. Lee, J. Zhang, H. Wang, D.P. Wilkinson, J. Appl. Electrochem. 36 (2006) 507–522.
[94] C.D. Squing, T.T. Cheng, M. Aindow, C. Erkey, Micropor. Mesopor. Mater. 80 (2005) 11–23.
[95] X. Dong, H. Hara, J. Fuel Cell Sci. Technol. 3 (2006) 477–481.
[96] N. Job, J. Marie, S. Lambert, S. Berthon-Fabry, P. Achard, Energy Convers. Manage. 49 (2008) 2461–2470.
[97] N. Rajalakshmi, H. Ryu, M.M. Shaijumon, S. Ramaprabhu, J. Power Sources 140 (2005) 250–257.
[98] T. Ioroi, H. Senoh, S.-i. Yamazaki, Z. Siroma, N. Fujiwara, K. Yasuda, J. Electrochem. Soc. 155 (2008) B321–B326.
[99] H. Chhina, S. Campbell, O. Kesler, J. Power Sources 179 (2008) 50–59.
[100] H. Chhina, S. Campbell, O. Kesler, J. Electrochem. Soc. 154 (2007) B533–B539.
[101] H. Chhina, S. Campbell, O. Kesler, J. Power Sources 161 (2006) 893–900.
[102] Y. Suzuki, A. Ishihara, S. Mitsushima, N. Kamiya, K. Ota, Electrochem. Solid-state Lett. 10 (2007) B105–B107.
[103] S. Maass, F. Finsterwalder, G. Frank, R. Hartmann, C. Merten, J. Power Sources 176 (2008) 444–451.
[104] M.L. Perry, T.W. Patterson, C. Reiser, ECS Trans. 3 (2006) 783–795.
[105] C.A. Reiser, D. Yang, R. Sawyer, U.S. Patent appl. 0076583 (2002).
[106] C.A. Reiser, D. Yang, R. Sawyer, U.S. Patent appl. 0134164 (2003).
[107] R.J. Balliet, C.A. Reiser, U.S. Patent appl. 0001980 (2004).
[108] J.A.S. Bett, N.E. Cipollini, T.D. Jarvi, R.D. Breault, U.S. Patent appl. 0126644 (2004).
[109] E. Passalacqua, F. Lufrano, G. Squadrito, A. Patti, L. Giorgi, Electrochim. Acta 46 (2001) 799–805.
[110] F.-Y. Zhang, S.G. Advani, A.K. Prasad, M.E. Boggs, S.P. Sullivan, T.P. Beebe Jr., Electrochim. Acta 54 (2009) 4025–4030.
[111] M. Aoki, H. Uchida, M. Watanabe, ECS Trans. 3 (2006) 485–492.
[112] J. Hou, W. Song, H. Yu, Y. Fu, L. Hao, Z. Shao, B. Yi, J. Power Sources 176 (2008) 118–121.
[113] A.P. Saab, F.H. Garzon, T.A. Zawodzinski, J. Electrochem. Soc. 149 (2002) A1541–A1546.
[114] A.P. Saab, F.H. Garzon, T.A. Zawodzinski, J. Electrochem. Soc. 150 (2003) A214–A218.
[115] F. Rong, C. Huang, Z.-S. Liu, D. Song, Q. Wang, J. Power Sources 175 (2008) 712–723.
[116] S. Kundu, M.W. Fowler, L.C. Simon, S. Grot, J. Power Sources 157 (2006) 650–656.
[117] Z. Qi, H. Tang, Q. Guo, B. Du, J. Power Sources 161 (2006) 864–871.
[118] M. Fouler, L.C. Simon, R. Abouatallah, J. Power Sources 182 (2008) 254–258.
[119] M. Oszcipok, M. Zedda, D. Riemann, D. Geckeler, J. Power Sources 154 (2006) 404–411.
[120] S. Ge, C.Y. Wang, Electrochim. Acta 52 (14) (2007) 4825–4835.
[121] X.G. Yang, Y. Tabuchi, F. Kagami, C.-Y. Wang, J. Electrochem. Soc. 155 (2008) B752–B761.
[122] Q. Yan, H. Toghiani, Y.-W. Lee, K. Liang, H. Causey, J. Power Sources 160 (2006) 1242–1250.
[123] R. Alink, D. Gerteisen, M. Oszcipok, J. Power Sources 182 (2008) 175–187.
[124] E. Cho, J.-J. Ko, H.Y. Hong, J. Electrochem. Soc. 150 (2003) A1667–A1670.
[125] R. Mukundan, Y.S. Kim, F. Garzon, B. Pivovar, ECS Trans. 1 (2006) 403–413.
[126] S. Kim, B.K. Ahn, M.M. Mench, J. Power Sources 179 (2008) 140–146.
[127] J. Hou, H. Yu, S. Zhang, S. Sun, H. Wang, B. Yi, P. Ming, J. Power Sources 162 (2006) 513–520.